Electroweak structure of the nucleon, meson cloud, and light-cone wave functions

B. Pasquini and S. Boffi

Dipartimento di Fisica Nucleare e Teorica, Università degli Studi di Pavia and INFN, Sezione di Pavia, Pavia, Italy

(Received 19 July 2007; published 15 October 2007)

The meson-cloud model of the nucleon consisting of a system of three valence quarks surrounded by a meson cloud is applied to study the electroweak structure of the proton and neutron. Light-cone wave functions are derived for the dressed nucleon as pictured to be part of the time a bare nucleon and part of the time a baryon-meson system. Configurations are considered where the baryon can be a nucleon or a Δ and the meson can be a pion as well as a vector meson such as the ρ or the ω. An overall good description of the electroweak form factors is obtained. The contribution of the meson cloud is small and only significant at low Q^2. Mixed-symmetry S'-wave components in the wave function are most important to reproduce the neutron electric form factor. Charge and magnetization densities are deduced as a function of both the radial distance from the nucleon center and the transverse distance with respect to the direction of the three-momentum transfer. In the latter case, a central negative charge is found for the neutron. The up and down quark distributions associated with the Fourier transform of the axial form factor have opposite sign, with the consequence that the probability to find an up (down) quark with positive helicity is maximal when it is (anti)aligned with the proton helicity.

DOI: 10.1103/PhysRevD.76.074011 PACS numbers: 12.39.−x, 13.40.Gp, 14.20.Dh

I. INTRODUCTION

Since the discovery of the proton finite size by Hofstadter and co-workers more than 50 years ago [1], electromagnetic form factors have played a privileged role in the investigation of the nucleon structure (for recent reviews, see [2–6]).

In principle, these quantities reflect the strong interaction between quarks inside the nucleon and should be described by quantum chromodynamics (QCD). In recent years important progress has been made with lattice QCD simulations [7–11]. Generic features of the baryon octet mass spectrum are reproduced well in quenched lattice QCD simulations (in which sea-quark contributions are neglected) and electromagnetic properties can be studied with pion masses as low as 0.3 GeV [10]. Qualitative agreement with the experimental data has been obtained [7,8], e.g. the flavor dependence of the Dirac form factor $F_1(Q^2)$ [12]. The isovector nucleon form factors were calculated in both the quenched and unquenched approximations with configurations for pion masses down to 380 MeV [9]. Small unquenching effects and results larger than the experimental data were found. Evaluating the axial form factors as well as the πNN and $\pi N\Delta$ form factors, it was possible to check the Goldberger-Treiman relations [13]. Qualitatively consistent results with experiment were obtained for the isovector form factor ratio $G_P(Q^2)/G_A(Q^2)$ of the nucleon axial vector form factors [11]. At present, the state of the art is still limited by systematic errors which are related to the fact that calculations are performed on finite volumes, at finite lattice spacings, and at quark masses which are still relatively large. In addition, the extrapolation to the chiral limit with the help of the chiral effective field theory requires calculations of higher order than presently available [14–16] (see also [17]) in order to account for the nonanalytic behavior of the form factors on the quark masses [18].

Therefore, model calculations are still a valuable tool for understanding the internal dynamics of the nucleon. In particular, many theoretical calculations have been done to investigate possible interpretations of the decreasing ratio of the proton electric to magnetic form factors, $\mu_p G_E^p(Q^2)/G_M^p(Q^2)$, as a function of Q^2 (see, e.g., [19] for an overview and [20,21] for the two-photon physics in elastic electron scattering), and we refer the reader to Refs. [4,5] for a discussion of the different interpretations of nucleon electromagnetic form factors proposed in the literature.

Here we want to consider the possibility that the physical nucleon is a bare nucleon surrounded by a meson cloud as a consequence of the spontaneously broken chiral symmetry. As first discussed in the context of deep inelastic scattering [22,23], a pion cloud can give an explanation of the flavor-symmetry violation in the sea-quark distributions of the nucleon thus accounting for the violation of the Gottfried sum rule [24]. This cloud will manifest itself as an extension of the charge distribution of protons and neutrons, which should be observable in the electromagnetic form factors at relatively small values of Q^2. In fact, the neutron charge density extracted from available data shows a positive core surrounded by a negative surface charge, peaking at just below 1 fm, which can be attributed to a negative pion cloud [25]. This is confirmed by the analysis of Ref. [26] showing a pronounced bump structure in the neutron electric charge form factor $G_E^n(Q^2)$ (and a dip in the other nucleon form factors) around $Q^2 = 0.2$–0.3 GeV^2, which can be interpreted as a signature of a very long-range contribution of the pion cloud extending out to 2 fm. It must be said, however, that from dispersion relation analysis [27,28] the pion cloud should peak much

more inside the nucleon, at $\sim$0.3 fm, and the desired bump-dip structure of Ref. [26] can only be achieved at the cost of low-mass poles close to the ω mass in the isoscalar channel and to the three-pion threshold in the isovector channel [29]. In addition, while confirming the long-range positively (negatively) charged component of the proton (neutron) charge density, a recent model-independent analysis of the infinite-momentum-frame charge density of partons in the transverse plane [30] is suggesting that the neutron parton charge density is negative at the center.

Mesonic degrees of freedom are naturally taken into account in the baryon chiral perturbation theory that is the effective field theory of the standard model at low energies and small momentum transfer. The electromagnetic form factors of the nucleon have been calculated to fourth order (one-loop) in baryon chiral perturbation theory within the manifestly Lorentz-invariant infrared regularization approach [31] and the extended on-mass-shell renormalization scheme [32,33]. The inclusion of vector mesons as explicit degrees of freedom results in a considerably improved description, accurate up to $Q^2 \simeq 0.4$ GeV^2.

The problem of considering the meson cloud surrounding a system of three valence quarks has been addressed already in the past in a variety of papers (see, e.g., [34–42] and references therein). Along the lines originally proposed in Refs. [43–45] and developed in [35], in this paper a baryon-meson Fock-state expansion is used to construct the state $|\tilde{N}\rangle$ of the physical nucleon. In the one-meson approximation the state $|\tilde{N}\rangle$ is pictured as being part of the time a bare nucleon, $|N\rangle$, and part of the time a baryon-meson system, $|BM\rangle$. The bare nucleon is formed by three valence quarks identified as constituent quarks according to the ideas discussed in [46]. The model was revisited in Ref. [47] to study generalized parton distributions where the meson cloud gives an essential contribution in the so-called ERBL region. We apply here the model to calculate the electroweak form factors of the nucleon. The baryon-meson system is assumed to include configurations where the baryon can be a nucleon or a Delta and the meson can be a pion as well as a vector meson such as the ρ or the ω.

In Sec. II the relevant formulas of the meson-cloud model are collected and the light-cone wave functions derived. The calculation of the electroweak form factors of the proton and neutron is illustrated in Sec. III, and the results are presented and discussed in Sec. IV. Concluding remarks are collected in the final section. Technical details necessary to calculate the vertex functions describing the transition to a baryon-meson state with vector mesons are given in the Appendix.

II. LIGHT-CONE WAVE FUNCTION OF THE NUCLEON IN THE MESON-CLOUD MODEL

The derivation of the nucleon light-cone wave function (LCWF) in the meson-cloud model has been already discussed in Ref. [47]. In this section we review some pertinent formulas necessary for the calculation of the form factors. In the meson-cloud model the nucleon is viewed as a quark core, termed the bare nucleon, surrounded by a meson cloud. The mesonic effects are treated perturbatively, by truncating the Fock-space expansion of the nucleon state to the dominant components given by the bare nucleon and the state containing a virtual meson with a recoiling baryon. The corresponding quantum state of the physical nucleon ($\tilde{N}$), with four-momentum $p_N^\mu = (p_N^-, p_N^+, \mathbf{p}_{N\perp}) \equiv (p_N^-, \tilde{p}_N)$ and helicity λ, can be written as

$$|\tilde{p}_N, \lambda; \tilde{N}\rangle = \sqrt{Z}|\tilde{p}_N, \lambda; N\rangle + \sum_{B,M} \int \frac{dy d^2\mathbf{k}_\perp}{2(2\pi)^3} \frac{1}{\sqrt{y(1-y)}} \sum_{\lambda',\lambda''} \phi^{\lambda(N,BM)}_{\lambda'\lambda''}(y, \mathbf{k}_\perp) |y p_N^+, \mathbf{k}_\perp + y\mathbf{p}_{N\perp}, \lambda'; B\rangle \times |(1-y)p_N^+, -\mathbf{k}_\perp + (1-y)\mathbf{p}_{N\perp}, \lambda''; M\rangle, \quad (1)$$

where the function $\phi^{\lambda(N,BM)}_{\lambda'\lambda''}(y, \mathbf{k}_\perp)$ is the probability amplitude to find a physical nucleon with helicity λ in a state consisting of a virtual baryon B and a virtual meson M, with the baryon having helicity λ', longitudinal-momentum fraction y, and transverse momentum $\mathbf{k}_\perp$, and the meson having helicity λ'', longitudinal-momentum fraction $1-y$, and transverse momentum $-\mathbf{k}_\perp$. From the normalization condition of the nucleon state

$$\langle \tilde{p}'_N, \lambda'; \tilde{N}|\tilde{p}_N, \lambda; \tilde{N}\rangle = 2(2\pi)^3 p_N^+ \delta(p'^+_N - p_N^+) \times \delta^{(2)}(\mathbf{p}'_{N\perp} - \mathbf{p}_{N\perp})\delta_{\lambda\lambda'}, \quad (2)$$

one obtains the following condition on the renormalization factor Z:

$$1 = Z + \sum_{B,M} P_{BM/N}, \quad (3)$$

with

$$P_{BM/N} = \int \frac{dy d^2\mathbf{k}_\perp}{2(2\pi)^3} \sum_{\lambda',\lambda''} |\phi^{1/2(N,BM)}_{\lambda'\lambda''}(y, \mathbf{k}_\perp)|^2. \quad (4)$$

From the definitions in Eqs. (3) and (4), one can interpret the factor Z as the probability of finding a bare nucleon in the physical nucleon, and $P_{BM/N}$ as the probability of fluctuation of the nucleon in a baryon-meson state.

The probability amplitude $\phi^{\lambda(N,BM)}_{\lambda'\lambda''}$ can be calculated using time-ordered perturbation theory in the infinite-momentum frame as explained in Ref. [47]. The final result

reads

$$\phi^{\lambda(N,BM)}_{\lambda'\lambda''}(y,\mathbf{k}_\perp)=\frac{1}{\sqrt{y(1-y)}}\frac{V^{\lambda}_{\lambda',\lambda''}(N,BM)}{M_N^2-M_{BM}^2(y,\mathbf{k}_\perp)}, \quad (5)$$

where $V^{\lambda}_{\lambda',\lambda''}(N,BM)$ is the vertex function describing the transition of the nucleon into a baryon-meson state, with squared invariant mass

$$M_{BM}^2(y,\mathbf{k}_\perp)\equiv\frac{M_B^2+\mathbf{k}_\perp^2}{y}+\frac{M_M^2+\mathbf{k}_\perp^2}{1-y}. \quad (6)$$

The vertex function $V^{\lambda}_{\lambda',\lambda''}(N,BM)$ has the following general expression [48]:

$$V^{\lambda}_{\lambda',\lambda''}(N,BM)=\bar{u}_{N\alpha}(\tilde{p}_N,\lambda)\upsilon^{\alpha\beta\gamma}\chi_\beta(\tilde{p}_M,\lambda'')\psi_\gamma(\tilde{p}_B,\lambda'), \quad (7)$$

where u_N is the nucleon spinor, χ and ψ are the field operators of the intermediate meson and baryon, respectively, and α, β, γ are bispinor and/or vector indices depending on the representation used for particles of given type. The explicit expressions for the πN and $\pi\Delta$ cases have been derived in Appendix C of Ref. [47], while the corresponding results for transitions with vector mesons are worked out in the Appendix. Because of the extended structure of the hadrons involved, one has also to multiply the coupling constant for pointlike particles in the interaction operator $\upsilon^{\alpha\beta\gamma}$ by phenomenological vertex form factors. These form factors parametrize the unknown microscopic effects at the vertex and have to obey the constraint $F_{NBM}(y,k_\perp^2)=F_{NBM}(1-y,k_\perp^2)$ to ensure basic properties like charge and momentum conservation simultaneously [49]. To this aim we will use the following functional form:

$$F_{NBM}(y,k_\perp^2)=\exp\left[\frac{M_N^2-M_{BM}^2}{2\Lambda_{BM}}\right], \quad (8)$$

where Λ_{BM} is a cutoff parameter.

For the hadron states of the bare nucleon and baryon-meson components in Eq. (1), we adopt a light-cone constituent quark model, by using the minimal Fock-state wave function in the light-cone formalism, i.e.

$$|\tilde{p}_H,\lambda;H\rangle=\sum_{\tau_i,\lambda_i}\int\left[\frac{\mathrm{d}x}{\sqrt{x}}\right]_N[\mathrm{d}^2\mathbf{k}_\perp]_N\Psi^{H,[f]}_\lambda \times(\{x_i,\mathbf{k}_{\perp i};\lambda_i,\tau_i\}_{i=1,\ldots,N}) \times\prod_{i=1}^N|x_ip_H^+,\mathbf{p}_{i\perp},\lambda_i,\tau_i\rangle, \quad (9)$$

where $\Psi^{H,[f]}_\lambda(\{x_i,\mathbf{k}_{\perp i};\lambda_i,\tau_i\}_{i=1,\ldots,N})$ is the momentum LCWF which gives the probability amplitude for finding in the hadron N partons with momenta $(x_ip_H^+,\mathbf{p}_{i\perp}=\mathbf{k}_{i\perp}+x_i\mathbf{p}_{H\perp})$, and spin and isospin variables λ_i and τ_i, respectively. In Eq. (9) and in the following formulas, the integration measures are defined by

$$\left[\frac{\mathrm{d}x}{\sqrt{x}}\right]_N=\left(\prod_{i=1}^N\frac{\mathrm{d}x_i}{\sqrt{x_i}}\right)\delta\left(1-\sum_{i=1}^N x_i\right), \quad (10)$$

$$[\mathrm{d}^2\mathbf{k}_\perp]_N=\left(\prod_{i=1}^N\frac{\mathrm{d}^2\mathbf{k}_{\perp i}}{2(2\pi)^3}\right)2(2\pi)^3\delta\left(\sum_{i=1}^N\mathbf{k}_{\perp i}\right), \quad (11)$$

where the number of valence partons is $N=3$ and $N=2$ for the baryon and meson case, respectively. As explained in Ref. [50], the wave function $\Psi^{H,[f]}_\lambda$ can be obtained by transforming the ordinary equal-time (instant-form) wave function in the rest frame into that in the light-front dynamics, by taking into account relativistic effects such as the Melosh-Wigner rotation, i.e.

$$\Psi^{H,[f]}_\lambda(\{x_i,\mathbf{k}_{\perp i};\lambda_i,\tau_i\}_{i=,1,\ldots,N})=2(2\pi)^3\frac{1}{\sqrt{M_0}}\prod_{i=1}^N\left(\frac{\omega_i}{x_i}\right)^{1/2}\sum_{\mu_1,\ldots,\mu_N}\Psi^{H,[c]}_\lambda(\{\mathbf{k}_i;\mu_i,\tau_i,\mu_i\}_{i=1,\ldots,N})\prod_{i=1}^N D^{1/2*}_{\mu_i\lambda_i}(R_{cf}(\tilde{k}_i)), \quad (12)$$

where $\Psi^{H,[c]}_\lambda$ is the canonical wave function, and $D^{1/2*}_{\mu_i\lambda_i}(R_{cf}(\tilde{k}_i))$ are the Melosh rotations defined in Ref. [50]. In Eq. (12), $\omega_i=\sqrt{m^2+\mathbf{k}_i^2}$ is the energy of the ith quark, and $M_0=\sum_i\omega_i$ is the free mass of the system of N noninteracting quarks.

In our model calculation, we take into account the meson-cloud contribution corresponding to π, ρ, and ω, with the accompanying baryon in the $|BM\rangle$ component of the dressed nucleon being a nucleon or a Δ. The instant-form wave function is constructed as the product of a momentum wave function, which is spherically symmetric and invariant under permutations, and a spin-isospin wave function, which is uniquely determined by SU(6)-symmetry requirements.

In the case of the nucleon, we adopt the momentum wave function of Ref. [51], which reads

$$\psi^{N,[c]}(\{\mathbf{k}_i\}_{i=1,3})=\frac{N'}{(M_0^2+\beta^2)^\gamma}, \quad (13)$$

with N' a normalization factor. In Eq. (13), the scale β, the parameter γ for the power-law behavior, and the quark mass m are taken as free parameters, and will be determined by a comparison with experimental data as explained in Sec. IV.

The Δ is described as a state of isospin $T = 3/2$ obtained as a pure spin-flip excitation of the nucleon, with the corresponding momentum wave function equal to that of the nucleon in Eq. (13).

Furthermore, the canonical wave function of the pion is taken from Ref. [52] and reads

$$\psi^{\pi,[c]}(\vec{k}_1, \vec{k}_2) = \frac{i}{\pi^{3/4}\alpha^{3/2}} \exp[-k^2/(2\alpha^2)], \tag{14}$$

with $\vec{k} = \vec{k}_1 = -\vec{k}_2$, and the two parameters $\alpha = 0.3659$ GeV and $m_q = 0.22$ GeV fitted to the pion form factor data. The phase of the pion wave function (14) is consistent with that of the antiquark spinors of Ref. [53].

The wave function of the ρ differs from the pion only in the spin component, with the rest-frame spin states of the $q\bar{q}$ pair coupled to $J = 1$ instead of $J = 0$. Similarly, the ω is described by the same spin and momentum wave function as the ρ, but with the isospin component corresponding to a singlet state. This choice corresponds to assuming an ideal mixing in the vector sector, since the effects of the $\phi - \omega$ mixing are irrelevant in the calculation of the meson-cloud contribution to the nucleon form factors. For the same reason, also the effects of the $\rho^0 - \omega$ mixing are neglected.

Finally, we need to specify the parameters entering in the vertex functions. The cutoff Λ_{BM} in Eq. (8) should in principle be different for each BM component. However, the Jülich group [54] and Zoller [44] used high-energy particle production data to determine all the Λ_{BM} of interest, and found that the data could be described by two parameters: Λ_1 for octet baryons and pseudoscalar and vector mesons, and Λ_2 for decuplet baryons. We have chosen the values $\Lambda_1 = 0.61$ GeV and $\Lambda_2 = 0.81$ GeV, which are consistent with the ones adopted in the cloudy bag model [49] to obtain a good fit to both the violation of the Gottfried sum rule and the measured sea-quark contribution in the unpolarized parton distribution. For the NBM coupling constants at the interaction vertex, we used the numerical values given in Refs. [55,56] in the case of the π and the ρ. Instead, for the $NN\omega$ coupling, $g_{NN\omega}$, we used the result from the analysis of Ref. [57] about the ω contribution to the unpolarized antiquark distributions, which favors a much smaller value for $g_{NN\omega}$ than the one used to describe the nucleon scattering data. The numerical values for each of the BM states are summarized in Table I.

Finally, with the specified parameters, the probabilities for each of the BM components in the dressed nucleon are

TABLE I. Coupling constants at the NBM interaction vertex.

$\frac{g^2_{NN\pi}}{4\pi}$	$\frac{f^2_{N\Delta\pi}}{4\pi}$	$\frac{g^2_{NN\rho}}{4\pi^2}$	$f_{NN\rho}$	$\frac{f^2_{N\Delta\rho}}{4\pi}$	$\frac{g^2_{NN\omega}}{4\pi^2}$
13.6	11.08 GeV^{-2}	0.84	$6.1 g_{NN\rho}$	20.45 GeV^{-2}	8.1

$$P_{N\pi/p} = P_{p\pi^0/p} + P_{n\pi^+/p} = 3P_{p\pi^0/p} = 5.1\%,$$
$$P_{\Delta\pi/p} = P_{\Delta^{++}\pi^-/p} + P_{\Delta^+\pi^0/p} + P_{\Delta^0\pi^+/p} = 2P_{\Delta^{++}\pi^-/p} = 3.40\%,$$
$$P_{N\rho/p} = P_{p\rho^0/p} + P_{n\rho^+/p} = 3P_{p\rho^0/p} = 0.11\%,$$
$$P_{\Delta\rho/p} = P_{\Delta^{++}\rho^-/p} + P_{\Delta^+\rho^0/p} + P_{\Delta^0\rho^+/p} = 2P_{\Delta^{++}\rho^-/p} = 0.67\%,$$
$$P_{N\omega/p} = P_{p\omega/p} = 0.013\%.$$

III. ELECTROWEAK FORM FACTORS OF THE NUCLEON IN THE MESON-CLOUD MODEL

The Dirac and Pauli form factors $F_1(Q^2)$ and $F_2(Q^2)$ of the nucleon are given by the spin conserving and the spin-flip matrix elements of the vector current $J^+_V = J^0_V + J^3_V$:

$$F_1(Q^2) = \langle \tilde{p} + \tilde{q}, \tfrac{1}{2}|J^+_V|\tilde{p}, \tfrac{1}{2}\rangle, \tag{15}$$

$$(q_x + iq_y)F_2(Q^2) = 2M_N\langle \tilde{p} + \tilde{q}, -\tfrac{1}{2}|J^+_V|\tilde{p}, \tfrac{1}{2}\rangle, \tag{16}$$

where $Q^2 = -q^2$. As was first shown by Drell and Yan [59], the calculation of the form factors is conveniently done in a coordinate frame where $q^+ = 0$. In particular, we will use a symmetric frame where the nucleon momenta are given by

$$p_N = \left[\frac{M_N^2 + \mathbf{q}_\perp^2/4}{p_N^+}, p_N^+, -\frac{\mathbf{q}_\perp}{2}\right] \equiv \left[\frac{M_N^2 + \mathbf{q}_\perp^2/4}{p_N^+}, \tilde{p}_N\right],$$
$$p'_N = \left[\frac{M_N^2 + \mathbf{q}_\perp^2/4}{\tilde{p}_N^+}, p_N^+, +\frac{\mathbf{q}_\perp}{2}\right] \equiv \left[\frac{M_N^2 + \mathbf{q}_\perp^2/4}{p_N^+}, \tilde{p}'_N\right]. \tag{17}$$

With such a choice, the processes with vacuum pair production are suppressed, and the current matrix elements can be computed as a simple overlap of Fock-space wave functions, with all off-diagonal terms involving pair production or annihilation by the current or vacuum vanishing. In the present meson-cloud model, we need to consider the contributions from the diagonal overlap between the bare-nucleon state, on one side, and the BM components, on the other side. Furthermore, the electromagnetic current is a sum of one-body currents, $J^+ = \sum_{B,M} J^+_B + J^+_M$, which involves individual hadrons one at a time. This corresponds to assuming that there are no interactions among the particles in a multiparticle Fock state during the interaction with the photon. Therefore the external probe can scatter either on the bare nucleon, $|N\rangle$, or one of the constituents of the higher Fock states, $|BM\rangle$. As a result, the matrix elements of the electromagnetic current can be written as the sum of the following two contributions:

$$\langle \tilde{p}'_N, \lambda'_N, \tilde{N}|J^+_V|\tilde{p}_N, \lambda_N, \tilde{N}\rangle = ZI^N_{\lambda'_N,\lambda_N} + \delta I_{\lambda'_N,\lambda_N}. \quad (18)$$

In Eq. (18), I^N is the contribution from the bare nucleon corresponding to the diagram (a) in Fig. 1, and δI is the contribution from the BM Fock components of the physical nucleon. This last term can further be split into two contributions, with the active particle being the baryon ($\delta I^{(B'B)M}$) or the meson ($\delta I^{(M'M)B}$), i.e.

$$\delta I_{\lambda'_N,\lambda_N} = \sum_{B,B',M} \delta I^{(B'B)M}_{\lambda'_N,\lambda_N} + \sum_{M',M,B} \delta I^{(M'M)B}_{\lambda'_N,\lambda_N}. \quad (19)$$

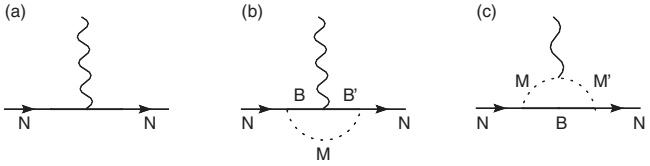

FIG. 1. Electromagnetic interaction vertex for a bare nucleon (a), and virtual baryon (b) and meson (c) components of a dressed nucleon.

The $\delta I^{(B'B)M}_{\lambda'_N,\lambda_N}$ term in Eq. (19) is schematically represented in Fig. 1(b) and is explicitly given by

$$\delta I^{(B'B)M}_{\lambda'_N,\lambda_N} = \sum_{B,B',M}\sum_{\lambda,\lambda',\lambda''}\int dy_B \int \frac{d^2\mathbf{p}_{B\perp}}{2(2\pi)^3}\langle \tilde{p}_B + \tilde{q}, \lambda', B'|J^+_B|\tilde{p}_B, \lambda, B\rangle \phi^{\lambda_N(N,BM)}_{\lambda''\lambda}(y_B, \mathbf{k}_{B\perp})[\phi^{\lambda'_N(N,B'M)}_{\lambda''\lambda'}(y_B, \mathbf{k}'_{B'\perp})]^*, \quad (20)$$

where $\mathbf{k}_{B\perp} = \mathbf{p}_{B\perp} - (1-y_B)\mathbf{q}_\perp/2$ and $\mathbf{k}'_{B'\perp} = \mathbf{p}_{B\perp} + (1-y_B)\mathbf{q}_\perp/2$.

Analogously, the contribution from the meson in the BM fluctuation is described by diagram (c) in Fig. 1 and reads

$$\delta I^{(M'M)B}_{\lambda'_N,\lambda_N} = \sum_{B,M,M'}\sum_{\lambda,\lambda',\lambda''}\int dy_M \int \frac{d^2\mathbf{p}_{M\perp}}{2(2\pi)^3}\langle \tilde{p}_M + \tilde{q}, \lambda', M'|J^+|\tilde{p}_M, \lambda, M\rangle \phi^{\lambda_N(N,BM)}_{\lambda''\lambda}(1-y_M, -\mathbf{k}_{M\perp}) \times [\phi^{\lambda'_N(N,BM')}_{\lambda''\lambda'}(1-y_M, -\mathbf{k}'_{M'\perp})]^*, \quad (21)$$

with $\mathbf{k}_{M\perp} = \mathbf{p}_{M\perp} - (1-y_M)\mathbf{q}_\perp/2$ and $\mathbf{k}'_{M'\perp} = \mathbf{p}_{M\perp} + (1-y_M)\mathbf{q}_\perp/2$.

As a result, the contribution from the BM components in Eqs. (20) and (21) is obtained by folding the current matrix elements of the baryon and meson constituents with the probability amplitudes describing the distributions of these constituents in the dressed initial and final nucleon. In general, the current matrix elements $\langle \tilde{p} + \tilde{q}|J^+|\tilde{p}\rangle$ appearing inside the integrals depend on the internal momentum of the baryon-meson state. However, as discussed in Ref. [60], the kinematical nature of a light-front boost allows us to transform these matrix elements to a frame with $\vec{p} = 0$, with the result

$$I_{\lambda'\lambda}(Q^2) = \langle \tilde{p} + \tilde{q}, \lambda'|J^+|\tilde{p}, \lambda\rangle = \langle M\mathbf{q}_\perp, \lambda|J^+|M\mathbf{0}_\perp, \lambda\rangle. \quad (22)$$

As a consequence, the current matrix elements in Eqs. (20) and (21) factor out of the internal momentum integration, and one finds

$$\delta I^{(B'B)M}_{\lambda'_N,\lambda_N} = \sum_{B,B',M}\sum_{\lambda,\lambda',\lambda''} I^{B'B}_{\lambda'\lambda}(Q^2) \times \int dy_B \int \frac{d^2\mathbf{p}_{B\perp}}{2(2\pi)^3}\phi^{\lambda_N(N,BM)}_{\lambda''\lambda}(y_B, \mathbf{k}_{B\perp}) \times [\phi^{\lambda'_N(N,B'M)}_{\lambda''\lambda'}(y_B, \mathbf{k}'_{B'\perp})]^*, \quad (23)$$

$$\delta I^{(M'M)B}_{\lambda'_N,\lambda_N} = \sum_{B,M,M'}\sum_{\lambda,\lambda',\lambda''} I^{M'M}_{\lambda'\lambda}(Q^2)\int dy_M \int \frac{d^2\mathbf{p}_{M\perp}}{2(2\pi)^3} \times \phi^{\lambda_N(N,BM)}_{\lambda''\lambda}(1-y_M, -\mathbf{k}_{M\perp}) \times [\phi^{\lambda'_N(N,BM')}_{\lambda''\lambda'}(1-y_M, -\mathbf{k}'_{M'\perp})]^*. \quad (24)$$

We also note that the sum in Eq. (19) over all the possible BM configurations leads to contributions from both the diagonal current matrix elements with the same hadrons in the initial and final state [$B' = B$ and $M' = M$ in Eqs. (23) and (24), respectively], and the current matrix elements involving the electromagnetic transition between different hadron states [i.e. the terms with $B' \neq B$ and $M' \neq M$ in Eqs. (23) and (24), respectively].

Finally, the current matrix element for the bare hadron states can be calculated as overlap integrals of the hadron LCWF (see, e.g., Refs. [53,61]):

$$\langle \tilde{p}'_{H'}, \lambda'_{H'}, H'|J^+_V|\tilde{p}_H, \lambda_H, H\rangle = \sum_j e_j \sum_{\lambda_i}\int [dx][d^2\mathbf{k}_\perp][\Psi^{H',[f]}_{\lambda'_{H'}}(\{x_i, \mathbf{k}'_{\perp i}; \lambda_i, \tau_i\}_{i=,1,\ldots,N})]^* \times \Psi^{H,[f]}_{\lambda_H}(\{x_i, \mathbf{k}_{\perp i}; \lambda_i, \tau_i\}_{i=,1,\ldots,N}), \quad (25)$$

where $\mathbf{k}'_{\perp j} = \mathbf{k}_{\perp j} + (1-x_j)\mathbf{q}_\perp$ for the struck quark, and $\mathbf{k}_{\perp i} = x_i\mathbf{q}_\perp$ for the spectator quarks.

The convolution formulas derived for the electromagnetic form factors can be extended to the calculation of the

proton axial form factor $G_A(Q^2)$. In this case we need to consider the diagonal matrix element of the axial current J_A^+, i.e.

$$G_A(Q^2) = \langle \tilde{p} + \tilde{q}, \tfrac{1}{2} | J_A^+ | \tilde{p}, \tfrac{1}{2} \rangle. \tag{26}$$

The structure of Eqs. (18), (19), (23), and (24) applies also for the axial matrix elements, with the difference that the active mesons in the $\delta I^{(M'M)B}$ contribution can only be vector mesons. Furthermore, the LCWF overlap representation of the axial matrix elements between bare hadron states reads

$$\langle \tilde{p}'_{H'}, \lambda'_{H'}, H' | J_A^+ | \tilde{p}_H, \lambda_H, H \rangle = \sum_j \tau_j \sum_{\lambda_i} \mathrm{sign}(\lambda_j) \int [\mathrm{d}x][\mathrm{d}^2\mathbf{k}_\perp] \times [\Psi^{H',[f]}_{\lambda'_{H'}}(\{x_i, \mathbf{k}'_{\perp i}; \lambda_i, \tau_i\}_{i=,1,\ldots,N})]^* \Psi^{H,[f]}_{\lambda_H}(\{x_i, \mathbf{k}_{\perp i}; \lambda_i, \tau_i\}_{i=,1,\ldots,N}). \tag{27}$$

IV. RESULTS AND DISCUSSION

As we are interested in studying the effects of the meson clouds that notoriously manifest themselves at low values of Q^2, the three free parameters of the model, β, γ in Eq. (13) and the quark mass m, are fixed by fitting 8 experimental values of the proton and neutron form factors at low Q^2. In the fit procedure we have used the Sachs form factors defined in terms of Dirac and Pauli form factors as

$$G_E(Q^2) = F_1(Q^2) - \frac{Q^2}{4M_N^2} F_2(Q^2), \qquad G_M(Q^2) = F_1(Q^2) + F_2(Q^2). \tag{28}$$

The electric form factors are normalized as usual, i.e. $G_E^p(0) = 1$, $G_E^n(0) = 0$, and the magnetic form factors at $Q^2 = 0$ are normalized to the nucleon magnetic moments, i.e. $G_M^{p,n}(0) = \mu^{p,n}$. We have chosen to fit μ^p, μ^n, the proton axial coupling constant $g_A = G_A(0)$, G_E^n at $Q^2 = 0.15$ GeV^2, and G_E^p and G_M^p at $Q^2 = 0.15$ and 0.45 GeV^2.

A 5% uncertainty was allowed in the fitting procedure. The multidimensional integration required for the numerical computation was implemented in a parallel computation using the parallelized version of the VEGAS routine of Ref. [62].

The fitted values are $\gamma = 3.21$, $\beta = 0.489$ GeV, and $m = 0.264$ GeV. These values differ from the original set of parameters in Ref. [51], used for the calculation of the nucleon electromagnetic form factors in a three-valence-quark model of the nucleon. They were fitted only to the anomalous magnetic moments of the proton and neutron to obtain $\gamma = 3.5$, $\beta = 0.607$ GeV, and $m = 0.263$ GeV.

In Table II the values of μ^p, μ^n, and g_A found in Ref. [51] are compared with those obtained here and the experimental values [58]. As in Ref. [51] and quite generally in the light-front formalism (see, e.g., Refs. [37,61,63–65]), it is always difficult to reproduce all the three quantities simultaneously, so that some compromise has to be accepted. A significant improvement is obtained for μ^n by taking into account the meson cloud. One may appreciate that the two contributions in the baryon-meson fluctuation with the active particle being a meson ($\sum_{B,B',M} \delta I^{(B'B)M}$) or a baryon ($\sum_{M,M',B} \delta I^{(M'M)B}$) add up coherently in the right direction bringing the values of μ^p, μ^n, and g_A closer to experiment.

The resulting electromagnetic form factors of both the proton and neutron are shown in Fig. 2 in comparison with the world data considered in the analysis of Ref. [26] and the recent JLab data [19]. A rather good fit is obtained in the proton case in the whole range of available data, while in the neutron case the fit is less satisfactory. In any case, the contribution from the meson cloud is smooth and mainly significant for $Q^2 < 0.5$ GeV^2 with a maximum at $Q^2 = 0$. Therefore, in agreement with dispersion relation analyses [27–29], this model is unable to produce the bump/dip structure advocated in Ref. [26] around $Q^2 = 0.2$–0.3 GeV^2. At higher Q^2 the explicit meson-cloud contribution dies out, but indirectly affects the bare nucleon contribution through the normalization factor Z [34], which is equal to 0.91 in our calculation.

TABLE II. Values of the form factors at $Q^2 = 0$ in the calculation of Ref. [51] (first column), from the bare nucleon contribution to the current matrix elements (second column), from the contribution of the baryon (third column) and meson (fourth column) state in the BM component of the dressed nucleon. The column labeled TOT gives the total result in the meson-cloud model, while in the last column (labeled Exp.) are given the experimental values.

	Ref. [51]	ZI^N	$\sum_{B,B',M} \delta I^{(B'B)M}$	$\sum_{M,M',B} \delta I^{(M'M)B}$	TOT	Exp. [58]
μ^p	2.78	2.52	0.18	0.17	2.87	2.793
μ^n	−1.69	−1.51	−0.12	−0.17	−1.80	−1.913
g_A	1.24	1.12	0.075	0.002	1.20	1.2670

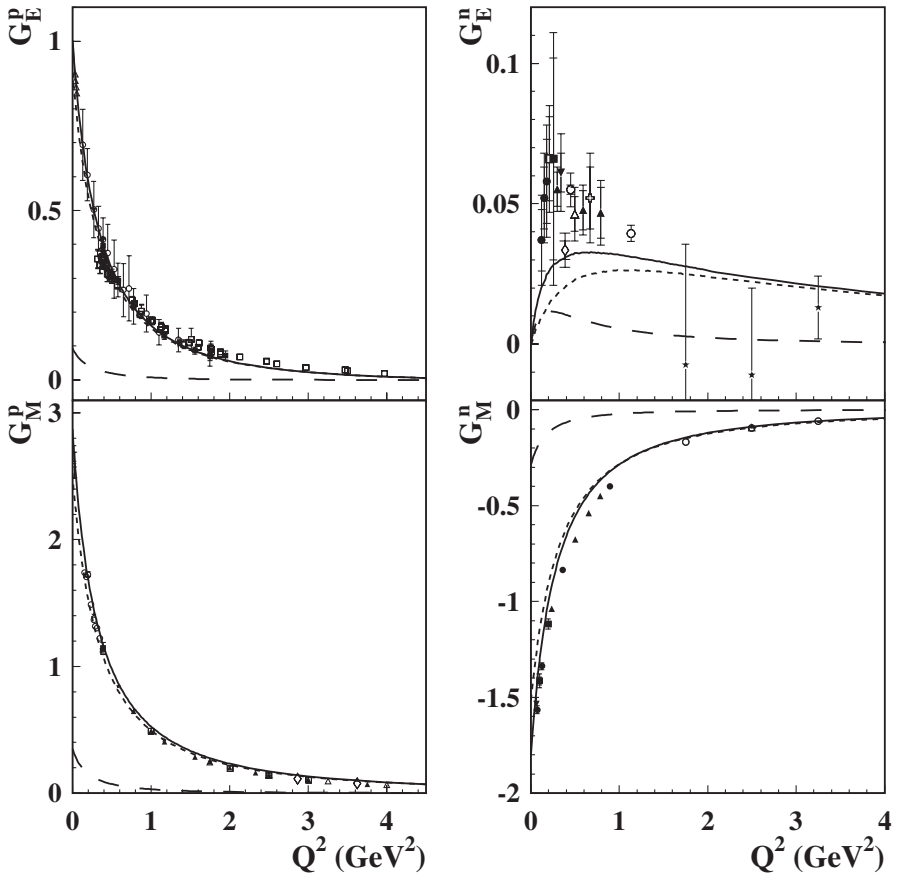

FIG. 2. The four nucleon electromagnetic form factors compared with the world data considered in the analysis of Ref. [26] and the recent JLab data [19] using $G_E^p = (\mu^p G_E^p/G_M^p)/(1 + Q^2/0.71\ \mathrm{GeV}^2)^2$ (open squares). Dotted (dashed) line for the contribution of the meson cloud (valence quarks). Solid line for the total result.

The results plotted in Fig. 2 are all obtained starting from an instant-form wave function $\Psi_\lambda^{H,[c]}$ in Eq. (12) containing a totally symmetric S-wave part in the quark momenta. In order to improve the result for the neutron electric form factor, it is known that the presence of a small admixture (1%–2%) of mixed-symmetry S'-wave components is most important [66–70]. Following [69], we assume the mixed-symmetry S'-wave component to be represented by an appropriate combination of mixed-symmetry spin-isospin wave functions with two radial wave functions of mixed symmetry of the form

$$\Psi_s^{N,[c]}(\mathbf{p},\mathbf{q}) = \mathcal{N}_s \frac{p^2 - q^2}{p^2 + q^2} \Psi^{N,[c]}(\{\mathbf{k}_i\}_{i=1,3}),$$
$$\Psi_a^{N,[c]}(\mathbf{p},\mathbf{q}) = \mathcal{N}_a \frac{\mathbf{p}\cdot\mathbf{q}}{p^2 + q^2} \Psi^{N,[c]}(\{\mathbf{k}_i\}_{i=1,3}), \tag{29}$$

where $\Psi^{N,[c]}(\{\mathbf{k}_i\}_{i=1,3})$ is the symmetric S-wave function (13), $\mathcal{N}_s$ and $\mathcal{N}_a$ are normalization factors, and $\mathbf{p}$ and $\mathbf{q}$ are the Jacobi coordinates:

$$\mathbf{p} = -\sqrt{\tfrac{3}{2}}(\mathbf{k}_1 + \mathbf{k}_2), \qquad \mathbf{q} = \sqrt{\tfrac{1}{2}}(\mathbf{k}_1 - \mathbf{k}_2). \tag{30}$$

The consequences of including a small percentage of such mixed-symmetric contribution to the neutron electric form factor are illustrated in Fig. 3. Even a percentage as small as 1% is able to produce a quite good result compared to data. As anticipated in Ref. [69], the same calculation leaves the other nucleon form factors almost unaffected.

The slope of the electric form factor at $Q^2 = 0$ determines the nucleon charge radius, i.e.

$$r_{p,n}^2 = -6 \frac{\mathrm{d}G_E^{p,n}(Q^2)}{\mathrm{d}Q^2}\bigg|_{Q^2=0}. \tag{31}$$

The corresponding values for proton and neutron obtained using an SU(6) symmetric or a mixed-symmetric instant-form wave function are reported in Table III, where also the partial contributions are indicated when one considers either the bare nucleon or the contribution of the cloud with an active baryon or meson. Rather good values of r_p and r_n are obtained in the latter case. For the proton the charge radius is mostly due to the valence quarks, i.e. the bare proton. The meson cloud brings a contribution of about 5% which leads to a final value of 0.877 fm, in close agreement with the experimental value 0.8750 ± 0.0068 [58].

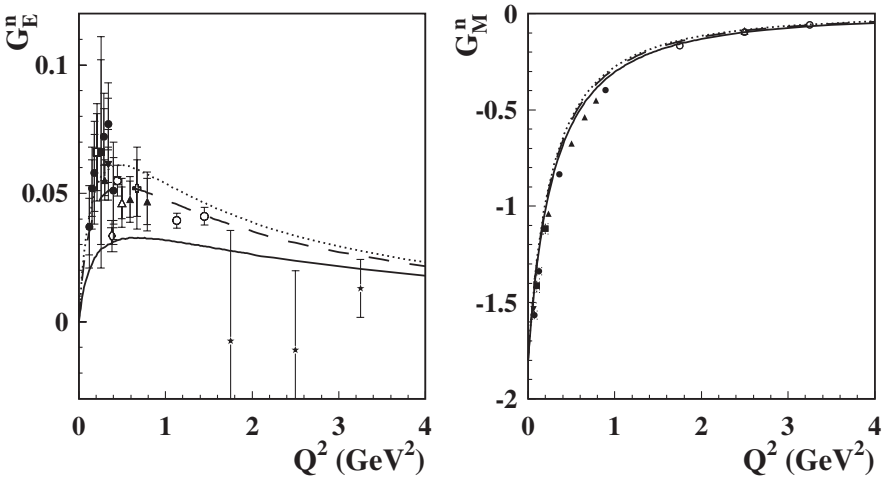

FIG. 3. The electric form factor of the neutron. Data points and solid line as in Fig. 2. Dashed (dotted) line with 1% (2%) mixed-symmetry S'-state in the bare neutron wave function.

TABLE III. The different contributions (in fm^2) to the proton and neutron mean square charge radii, r_p^2 and r_n^2 respectively, from the bare nucleon and when the baryon or the meson is active in the cloud. The column labeled TOT is the total result. The lines labeled SU(6) (mixed symmetry) refer to the symmetry of the bare nucleon wave function of the bare nucleon.

		Bare nucleon	Active baryon	Active meson	TOT
r_p^2	SU(6)	0.64	0.065	0.061	0.77
r_p^2	Mixed symmetry	0.70	0.065	0.061	0.82
r_n^2	SU(6)	−0.0097	0.0085	−0.063	−0.064
r_n^2	Mixed symmetry	−0.058	0.0085	−0.063	−0.112

Including the mixed-symmetry S'-wave component, the charge radius of the bare proton is 0.837 fm. The cloud adds a small contribution, which makes the total value slightly overestimated. In the neutron case the bare contribution is quite small, as expected. In contrast, both the cloud and the mixed symmetry are equally important. The contribution of the active meson in the cloud is substantial and with the right sign. Including also the mixed-symmetry S'-wave component r_n^2 becomes quite close to the experimental value -0.1161 ± 0.0022 [58].

In Fig. 4 the electric to magnetic form factor ratio $\mu^p G_E^p/G_M^p$ is shown for the proton. The model follows the observed trend of data taken in polarized elastic electron scattering with a steepest falloff at values of Q^2 much larger than those involved in the fit to determine the model parameters. This is due to the combined effect of a slightly overestimated G_M^p and a slightly underestimated G_E^p at large values of Q^2 (see Fig. 2), where in practice only the valence quarks contribute. The result is only slightly modified when including a mixed-symmetry contribution in the nucleon wave function.

The predicted axial form factor of the proton is shown in Fig. 5. The axial form factor has been normalized by its

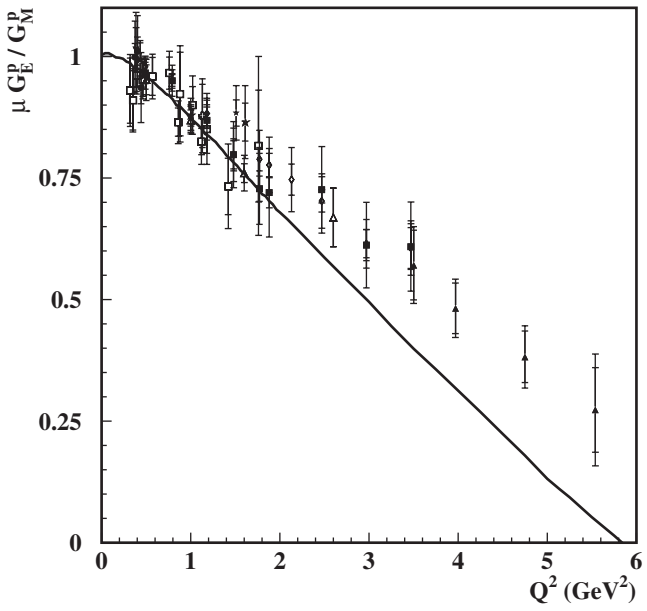

FIG. 4. The electric to magnetic form factor ratio $\mu^p G_E^p/G_M^p$ for the proton. Data points as in Fig. 2.

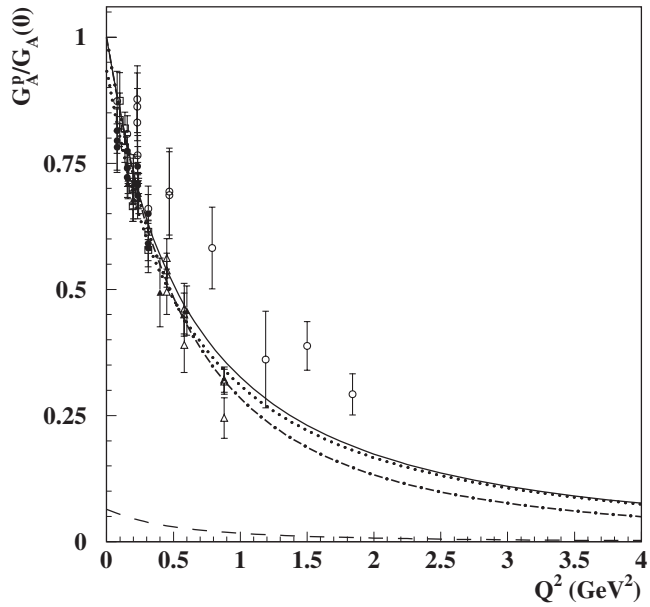

FIG. 5. The axial form factor of the proton. Dotted (dashed) line for the contribution of the meson cloud (valence quarks). Solid line for the total result. Dot-dashed line for the phenomenological dipole form. Data points are the world data considered in Ref. [71].

value at $Q^2 = 0$, i.e. by the fitted value of the axial coupling constant g_A. Also in this case the meson-cloud contribution is only significant at low values of Q^2, although not sufficient to bring g_A in complete agreement with experiment. However, the observed dipole form of the axial form factor, i.e. $G_A(Q^2)/G_A(0) = 1/(1 + Q^2/M_A^2)^2$ with $M_A = 1.069$ GeV, is well reproduced.

Neglecting relativistic corrections, in the Breit frame the radial distribution of the nucleon charge (ρ_{ch}) and magnetization (ρ_m) are given by the Fourier-Bessel transform of the nucleon electromagnetic Sachs form factors, i.e.

$$\rho_{ch}^{p,n}(r) = \frac{2}{\pi}\int \mathrm{d}QQ^2 j_0(Qr) G_E^{p,n}(Q^2), \tag{32}$$

$$\mu^{p,n}\rho_m^{p,n}(r) = \frac{2}{\pi}\int \mathrm{d}QQ^2 j_0(Qr) G_M^{p,n}(Q^2). \tag{33}$$

The corresponding results are shown in Fig. 6 together with the partial contributions from the bare nucleon and when the baryon or the meson is active in the cloud. In all cases, the meson-cloud contribution is rather smooth and dies out beyond 2 fm. With the exception of the neutron charge density, when the baryon is active its contribution is peaked

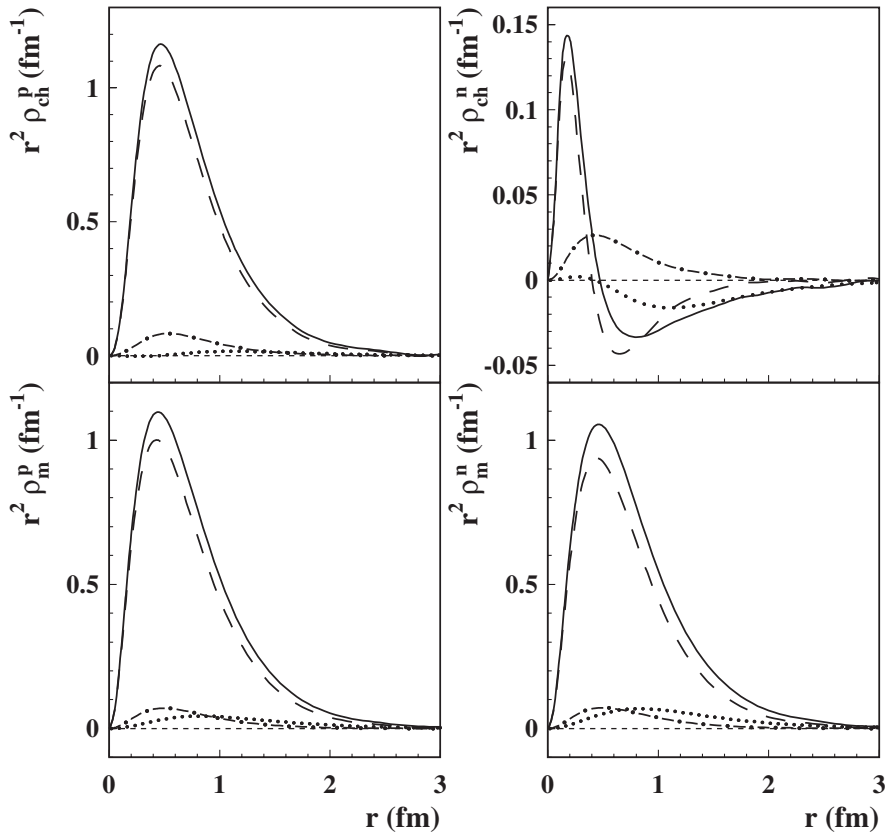

FIG. 6. The proton and neutron charge and magnetization densities. Dashed, dot-dashed, and dotted lines for contributions from the bare nucleon, the active baryon, and the active meson in the cloud. Solid line for the total result.

at approximately the same position as the bare-nucleon contribution, while the active meson is peaked at ~1 fm. Thus, the meson cloud manifests itself as a slight extension of the radial distribution up to ~2 fm as suggested by the analysis of Ref. [26]. In the case of the neutron charge distribution, the two components of the meson cloud behave differently. The active baryon, a proton or a Δ^+, gives a positive contribution of the same shape as the bare proton and is appropriately scaled by the corresponding vertex functions. The contribution of the active meson, a π^-, is opposite and peaked at ~1.3 fm. The resulting charge distribution shows a positive core surrounded by a negative surface charge pushed outwards by the meson cloud and peaking at ~0.8 fm, in agreement with the analysis of Ref. [25] and the expectation based on the picture of a hadron's periphery caused by the pion cloud [72].

The effect of including the mixed-symmetry S'-wave component in the neutron case can be appreciated from Fig. 7. The inner positive core is more pronounced and the negative surface charge is even more pushed outwards. Consequently, the (negative) mean square radius approaches the experimental value (see Table III).

The direct relationship between Sachs form factors and the static charge and magnetization densities is lost when relativity is considered because there is a variation with Q^2 of the Breit frame and electron scattering measures transitions matrix elements between nucleon states that have different momenta. Therefore one has to apply appropriate boosts that in a relativistic composite system such as the

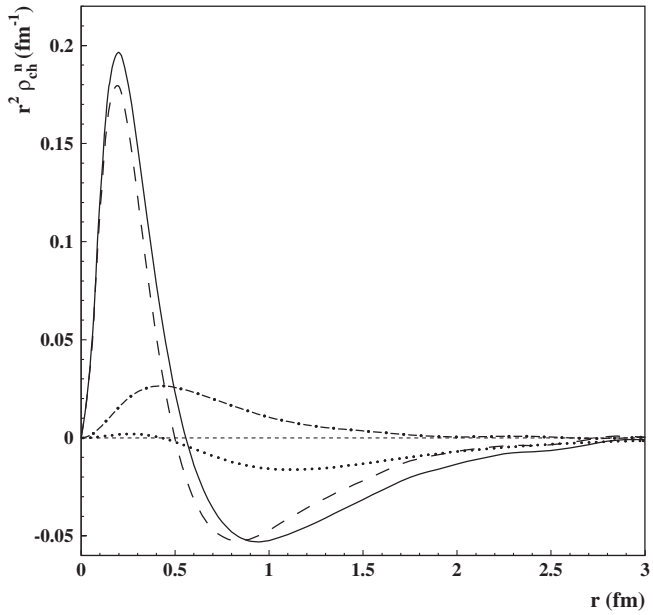

FIG. 7. The neutron charge density with a mixed-symmetry S'-wave component in the neutron wave function. Dashed, dot-dashed, and dotted lines for contributions from the bare nucleon, the active baryon, and the active meson in the cloud. Solid line for the total result.

nucleon depend on the interaction among its constituents. The problem of finding a suitable prescription to relate Sachs form factors to the static charge and magnetization densities was recently addressed in Ref. [25] taking into account the Lorentz contraction of the densities in the Breit frame relative to the rest frame. The consequences are that relativity tends to pull the density inward and to amplify oscillations at large radii. This has been confirmed in the model of Ref. [38]. The same effect should be expected also here. In any case in the present analysis the meson cloud is responsible for a long-range contribution to the nucleon charge and magnetization densities.

The problem of unambiguously determining the charge density can be solved by looking at the charge density $\rho(b)$ of partons in the transverse (impact parameter) plane with respect to the direction of the three-momentum transfer [30]. This is possible because in the transverse plane boosts are purely kinematical, i.e. in the light-front framework they form a Galilei subgroup of the Poincaré group [73,74]. Then $\rho(b)$ is the two-dimensional Fourier transform of the Dirac form factor F_1:

$$\rho(b) = \frac{1}{2\pi} \int_0^\infty \mathrm{d}QQJ_0(Qb)F_1(Q^2), \tag{34}$$

where J_0 is a cylindrical Bessel function.

The corresponding charge densities for the proton and the neutron are plotted in Fig. 8. As in Ref. [30] the densities are concentrated at low values of b with a positive peak for the proton and a negative peak for the neutron.

These nucleon charge densities can be related to quark transverse distributions. Assuming that only up and down quarks are in the nucleon and invoking isospin symmetry, we have

$$\rho^p(b) = \tfrac{4}{3}u(b) - \tfrac{1}{3}d(b), \tag{35}$$

$$\rho^n(b) = -\tfrac{2}{3}u(b) + \tfrac{2}{3}d(b), \tag{36}$$

where $u(b)$ is the transverse distribution for an up quark in the proton or a down quark in the neutron, and $d(b)$ is the transverse distribution for a down quark in the proton or an up quark in the neutron. Both $u(b)$ and $d(b)$ are normalized to 1. They can be obtained using

$$u(b) = \rho^p(b) + \tfrac{1}{2}\rho^n(b), \tag{37}$$

$$d(b) = \rho^p(b) + 2\rho^n(b). \tag{38}$$

The resulting distributions are shown in Fig. 9 in the two cases of a permutationally symmetric momentum wave function of the bare nucleon and of an included mixed-symmetric component. The central up quark density turns out to be larger than that of the down quark by about 40%

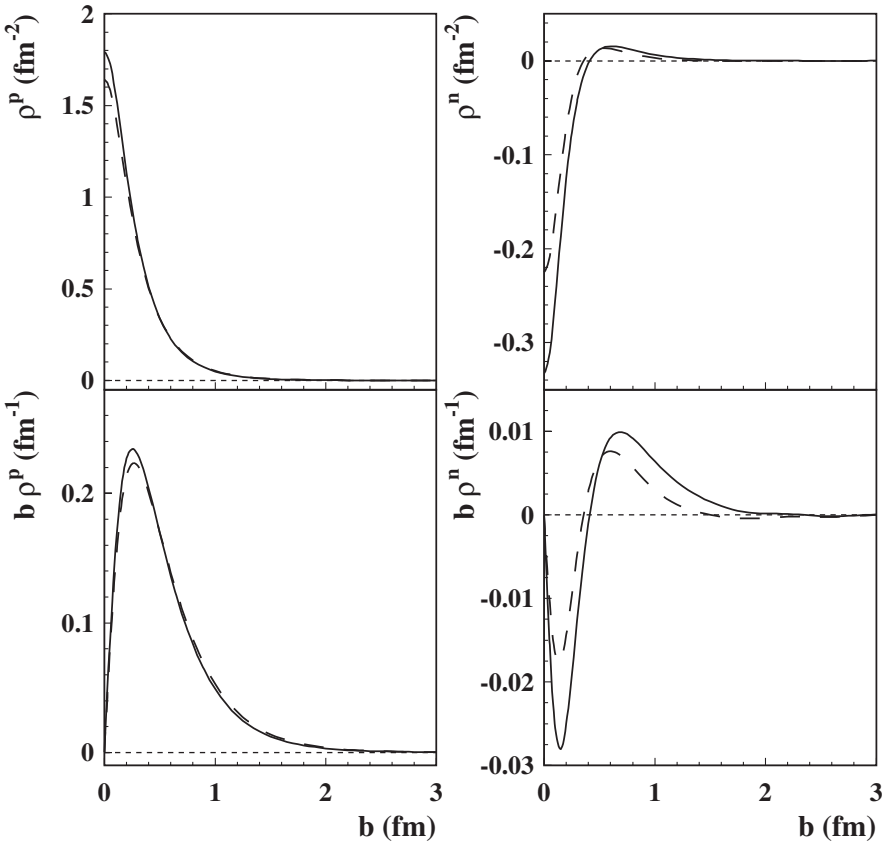

FIG. 8. The proton and neutron charge density as a function of the impact parameter b. Solid lines for a permutationally symmetric momentum wave function, dashed lines with mixed-symmetry components included.

in the symmetric case and by about 25% including the mixed symmetry. Quite similar results (about 30%) have been obtained in Ref. [30] using phenomenological parametrizations of the Sachs form factors and deducing F_1 in terms of G_E and G_M.

The probability $\rho^q(b, \lambda, \Lambda)$ to find a quark with transverse position b and light-cone helicity $\lambda(= \pm 1)$ in the nucleon with longitudinal polarization $\Lambda(= \pm 1)$ can be expressed as the Fourier transform of the combination of the quark contributions to the Dirac and axial form factors

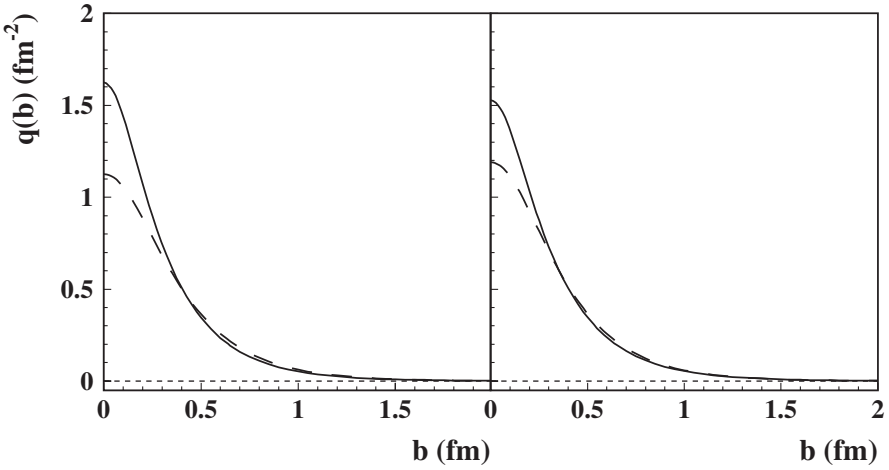

FIG. 9. Transverse distributions of up (solid lines) and down (dashed lines) quarks in the proton as a function of the impact parameter b with a permutationally symmetric momentum wave function of the bare nucleon (left panel), and with a mixed-symmetric component (right panel).

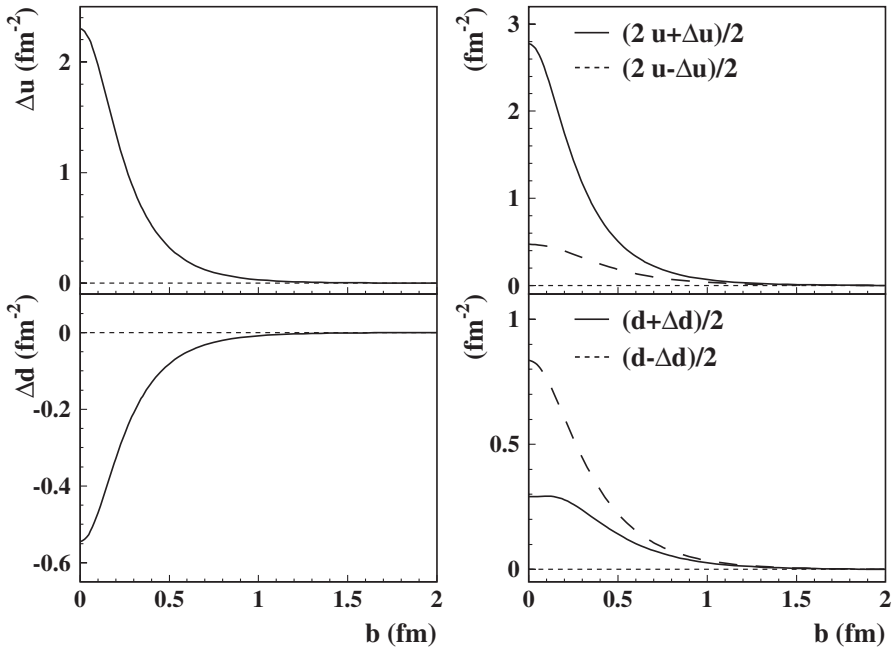

FIG. 10. Transverse distribution of up and down quarks in a longitudinally polarized proton as a function of the impact parameter b. Left panels: the axial contributions Δu and Δd for up and down quarks, respectively. Right panels: total contribution for quarks polarized in the longitudinal direction, either parallel (solid lines) or antiparallel (dashed lines) to the proton helicity.

[75], i.e.

$$\begin{aligned}\rho^q(b,\lambda,\Lambda) &= \frac{1}{2}\int \mathrm{d}^2\mathbf{q}_\perp [F_1^q(Q^2=\mathbf{q}_\perp^2) \\ &\quad + \lambda\Lambda G_A^q(Q^2=\mathbf{q}_\perp^2)]e^{i\mathbf{q}_\perp\cdot\mathbf{b}} \\ &= \frac{1}{4\pi}\int \mathrm{d}Q Q J_0(Qb)[F_1^q(Q^2)+\lambda\Lambda G_A^q(Q^2)] \\ &\equiv \frac{1}{2}[\rho^q(b)+\lambda\Lambda\Delta q(b)], \end{aligned} \tag{39}$$

where $\rho^q(b)$ was already defined in Eq. (38) and $\Delta q(b)$ is the Fourier transform of $G_A^q(Q^2)$. Assuming a positive proton helicity ($\Lambda = 1$), the resulting probability is shown in the right panels of Fig. 10. The axial contributions $\Delta u(b)$ and $\Delta d(b)$ for up and down quarks (left panels), respectively, have opposite sign. When suitably combined with the corresponding transverse distributions $u(b)$ and $d(b)$ given in Fig. 9, we see that the positive helicity up quarks in the proton are preferentially aligned with the proton helicity, while the opposite occurs for down quarks. This result is in total agreement with that shown in Fig. 7 of Ref. [75], where quite a different radial distribution of the axially symmetric spin density was presented for up and down quarks in the transverse plane.

V. CONCLUDING REMARKS

The meson-cloud model, as revisited in Ref. [47] to study generalized parton distributions and including baryon-meson configurations with the baryon being a nucleon or a Δ and the meson being a pion as well as a vector meson such as the ρ or the ω, has been used to describe the electroweak structure of the nucleon. Light-cone wave functions for the bare nucleon were constructed starting from the momentum wave function (13) taken from Ref. [51] and depending on three parameters, the scale β, the parameter γ for the power-law behavior, and the quark mass m. They are determined by fitting 8 experimental values of the proton and neutron form factors at low Q^2. No other free parameters enter the model calculations, since all other ingredients are fixed from the beginning on the basis of previous analysis.

An overall good fit to the electromagnetic form factors is obtained, with the exception of the neutron electric form factor where it is essential to also include a mixed-symmetry S'-wave momentum component, in agreement with earlier findings [66–70]. This component only slightly affects the other form factors. In any case, the meson-cloud contribution is smooth and only significant below $Q^2 = 0.5$ GeV^2. Therefore, as in analyses based on dispersion relations [27–29], also in this model no possibility exists to reproduce the bump/dip structure discussed in Ref. [26]. A similar smooth contribution arises in the proton axial form factor.

Charge and magnetization densities are deduced as a function of both the radial distance from the nucleon center and the transverse distance (impact parameter) with respect to the direction of the three-momentum transfer.

The meson cloud produces a slight extension of the radial distribution of the static charge and magnetization

up to ~2 fm. It is confirmed that the neutron charge distribution shows a positive core surrounded by a negative surface charge [25,30]. It is pushed outwards by the long-range meson cloud with opposite contributions from the active baryon and meson in the baryon-meson component of the nucleon wave function.

As a function of the impact parameter a central negative charge is found for the neutron. A similar result has been obtained in Ref. [30] starting from a phenomenological fit of the electromagnetic form factors. This result can be explained invoking isospin symmetry and observing that the up quark transverse distribution in the proton is larger than the down quark one, a result consistent with deep inelastic scattering data.

The up and down quark distributions associated with the Fourier transform of the axial form factor have opposite sign, with the consequence that the probability to find an up (down) quark with positive helicity is maximal when it is (anti)aligned with the proton helicity, in close agreement with the radial distribution of the axially symmetric spin density studied in Ref. [75].

In conclusion, the meson-cloud model appears to give a satisfactory description of the electroweak properties of the nucleon with interesting information about its structure in the nonperturbative regime of QCD.

ACKNOWLEDGMENTS

This research is part of the EU Integrated Infrastructure Initiative Hadron Physics Project under Contract No. RII3-CT-2004-506078. The diagrams in the paper have been drawn using the Jaxodraw package [80].

APPENDIX: VERTEX FUNCTIONS

In this Appendix we work out the case of the $B \to B'V$ transitions in the light-front formalism, with the baryon states B being a nucleon or a Δ, and the vector mesons V corresponding to ω, or ρ. The vertex functions for the coupling of baryons with pseudoscalar mesons are given in Appendix C of Ref. [47]. The vertex functions for transitions to vector mesons can be found in several places (see, e.g., Refs. [35,48,54]), and the longitudinal-momentum distributions corresponding to the integration over the transverse momentum of the squared vertex functions are explicitly given in Refs. [76–78]. The quoted results are controversial, in the sense that they differ although the formalism is exactly the same. In particular, we agree with the results for the longitudinal-momentum distributions of Refs. [77,78], and differ from Ref. [76], while for the vertex functions we agree with the conclusions drawn in the Appendix of Ref. [78], where the origin of the differences from Refs. [35,48,54] is explained in details. However, Kumano *et al.* [78] do not give explicit analytical expressions for the vertex functions, and we find convenient to show here their derivation and, in particular, their dependence on the transverse momentum which enters in the convolution formulas for the form factors.

The light-front vectors are defined as

$$A^\mu = (A^-, A^+, \mathbf{A}_\perp), \tag{A1}$$

with

$$A^\pm = A^0 \pm A^3, \qquad \mathbf{A}_\perp = (A^1, A^2). \tag{A2}$$

We also use the notations $A_{R,L} = A^1 \pm iA^2$ and $\tilde{A} = (A^+, \mathbf{A}_\perp)$.

The light-front nucleon spinors $u_\lambda(\tilde{p})$ are given by

$$\begin{aligned} u_{1/2}(\tilde{p}) &= \frac{1}{\sqrt{2p^+}} \begin{pmatrix} p^+ + m \\ p_R \\ p^+ - m \\ p_R \end{pmatrix}, \\ u_{-1/2}(\tilde{p}) &= \frac{1}{\sqrt{2p^+}} \begin{pmatrix} -p_L \\ p^+ + m \\ p_L \\ m - p^+ \end{pmatrix}. \end{aligned} \tag{A3}$$

The gamma matrices are defined as in Ref. [79].

A similar expansion for the Δ field involves the Rarita-Schwinger spinors given by

$$\begin{aligned} u^\mu_{3/2}(\tilde{p}) &= \epsilon^\mu_{+1}(\tilde{p}) u_{1/2}(\tilde{p}), \\ u^\mu_{1/2}(\tilde{p}) &= \sqrt{\tfrac{2}{3}}\epsilon^\mu_0(\tilde{p}) u_{1/2}(\tilde{p}) + \sqrt{\tfrac{1}{3}}\epsilon^\mu_{+1}(\tilde{p}) u_{-1/2}(\tilde{p}), \\ u^\mu_{-1/2}(\tilde{p}) &= \sqrt{\tfrac{2}{3}}\epsilon^\mu_0(\tilde{p}) u_{-1/2}(\tilde{p}) + \sqrt{\tfrac{1}{3}}\epsilon^\mu_{-1}(\tilde{p}) u_{1/2}(\tilde{p}), \\ u^\mu_{-3/2}(\tilde{p}) &= \epsilon^\mu_{-1}(\tilde{p}) u_{-1/2}(\tilde{p}), \end{aligned} \tag{A4}$$

where the polarization vectors are given by

TABLE IV. Vertex functions for $N \to N'V$ and particle helicities $\frac{1}{2} \to \lambda'_N$, λ_V in prescription A.

λ'_N	λ_V	$V(N, NV)$
$+\frac{1}{2}$	$+1$	$\frac{\sqrt{2}k_L}{\sqrt{y}}\left[\frac{g}{1-y} + \frac{f}{2}\right]$
$-\frac{1}{2}$	$+1$	$g\frac{\sqrt{2}(M_B - yM_N)}{\sqrt{y}} - \frac{f}{2M_N}\frac{\sqrt{2}[yM_V^2 - (1-y)^2 M_N M_B]}{\sqrt{y}(1-y)}$
$\frac{1}{2}$	0	$g\frac{(1-y)^2 M_N M_B - yM_V^2 + k_\perp^2}{M_V\sqrt{y}(1-y)} - \frac{f}{2M_N}\frac{M_V(yM_N - M_B)}{\sqrt{y}}$
$-\frac{1}{2}$	0	$g\frac{k_R(M_B - M_N)}{M_V\sqrt{y}} - \frac{f}{2M_N}\frac{k_R M_V(1+y)}{\sqrt{y}(1-y)}$
$+\frac{1}{2}$	-1	$-g\frac{\sqrt{2}yk_R}{\sqrt{y}(1-y)} + \frac{f}{2M_N}\frac{\sqrt{2}k_R M_B}{\sqrt{y}}$
$-\frac{1}{2}$	-1	$-\frac{f}{2M_N}\frac{\sqrt{2}k_R^2}{\sqrt{y}(1-y)}$

TABLE V. Vertex functions for $N \to N'V$ and particle helicities $\frac{1}{2} \to \lambda'_N$, λ_V in prescription B.

λ'_N	λ_V	$V(N, NV)$
$+\frac{1}{2}$	$+1$	$\frac{\sqrt{2}k_L}{\sqrt{y}}\left[\frac{g}{1-y}+\frac{f}{2}\right]$
$-\frac{1}{2}$	$+1$	$g\frac{\sqrt{2}(M_B-yM_N)}{\sqrt{y}}+\frac{f}{2M_N}\frac{\sqrt{2}[k_\perp^2-(M_N+M_B)(1-y)(yM_N-M_B)]}{\sqrt{y}(1-y)}$
$+\frac{1}{2}$	0	$g\frac{k_\perp^2+(1-y)^2M_NM_B-yM_V^2}{M_V\sqrt{y}(1-y)}+\frac{f}{2M_N}\frac{(yM_N-M_B)[k_\perp^2+y^2M_N^2-y(M_N^2+M_V^2+M_B^2)+M_B^2]}{2M_Vy\sqrt{y}}$
$-\frac{1}{2}$	0	$g\frac{(M_B-M_N)}{M_V\sqrt{y}}+\frac{f}{2M_N}\frac{k_R(1+y)[k_\perp^2-y(M_B^2+M_N^2+M_V^2)+M_B^2+y^2M_N^2]}{2M_Vy\sqrt{y}(1-y)}$
$+\frac{1}{2}$	-1	$-g\frac{\sqrt{2}yk_R}{\sqrt{y}(1-y)}+\frac{f}{2M_N}\frac{\sqrt{2}k_RM_B}{\sqrt{y}}$
$-\frac{1}{2}$	-1	$-\frac{f}{2M_N}\frac{\sqrt{2}k_R^2}{\sqrt{y}(1-y)}$

$$\epsilon^\mu_{+1}(\tilde{p})=\left(-\sqrt{2}\frac{p_R}{p^+},0,\left(-\frac{1}{\sqrt{2}},-\frac{i}{\sqrt{2}}\right)\right),$$
$$\epsilon^\mu_{0}(\tilde{p})=\frac{1}{m}\left(\frac{\mathbf{p}_\perp^2-m^2}{p^+},p^+,\mathbf{p}_\perp\right), \tag{A5}$$
$$\epsilon^\mu_{-1}(\tilde{p})=\left(\sqrt{2}\frac{p_L}{p^+},0,\left(\frac{1}{\sqrt{2}},-\frac{i}{\sqrt{2}}\right)\right).$$

The vertex function for the transition $N \to BV$ with the baryon B being one of the octet states is given by

$$V^{\lambda_N}_{\lambda'_B,\lambda_V}=\tilde{\phi}^*_V\cdot\tilde{T}F_{NBV}(y,k_\perp)\times\left[g\bar{u}(p'_B,\lambda'_B)\gamma^\mu u(p_N,\lambda_N)\varepsilon^*_{\mu,\lambda_V}-\frac{f}{2M_N}\bar{u}(p'_B,\lambda'_B)i\sigma^{\mu\nu}p_{\nu,V}\varepsilon^*_{\mu,\lambda_V}\right], \tag{A6}$$

where F_{NBV} is the vertex form factor, and the isospin factor is defined as

$$\langle B|\tilde{\phi}^*_V\cdot\tilde{T}|N\rangle=(-1)^{\tau_V}\frac{\langle T_B||\hat{T}||T_N\rangle}{\sqrt{2T_B+2}}\langle T_N\tau_N 1-\tau_V|T_B\tau_B\rangle, \tag{A7}$$

with $T_B=\frac{1}{2}$, and $\langle\frac{1}{2}\|\hat{T}\|\frac{1}{2}\rangle=\sqrt{6}$.

In the vertex function of Eq. (A6), there is an off-shell dependence introduced by the derivative coupling, leading to a freedom in defining the vertex momentum. One can consider the following two possibilities [54]:

$$\begin{aligned}&\text{(A)}\quad p_V^\nu=(E_V,\vec{p}_V),\quad \text{with } E_V=\sqrt{m_V^2+\vec{p}_V^2},\\ &\text{(B)}\quad p_V^\nu=p_N-p'_B=(E_N-E'_B,\vec{p}_V).\end{aligned} \tag{A8}$$

In the following we will list the results for the vertex functions corresponding to both prescriptions, although the calculation of the nucleon form factors is performed using the off-shell condition (B), as suggested in Ref. [54].

TABLE VI. Vertex functions for $N \to \Delta V$ and particle helicities $\frac{1}{2} \to \lambda'$, λ_V in prescription A.

λ'	λ_V	$V(N, NV)$
$+\frac{3}{2}$	$+1$	$-\frac{f}{M_V}\frac{k_L^2}{y\sqrt{y}(1-y)}$
$+\frac{3}{2}$	0	$\frac{f}{M_V}\frac{M_V\sqrt{2}k_L}{\sqrt{y}(1-y)}$
$+\frac{3}{2}$	-1	$\frac{f}{M_V}\frac{M_NM_B(1-y)^2-yM_V^2}{\sqrt{y}(1-y)}$
$+\frac{1}{2}$	1	$\frac{1}{\sqrt{3}}\frac{f}{M_V}\frac{k_L(k_\perp^2-2(1-y)M_B^2)}{M_By\sqrt{y}(1-y)}$
$+\frac{1}{2}$	0	$-\sqrt{\frac{2}{3}}\frac{f}{M_V}\frac{M_V[k_\perp^2-(1-y)M_B(M_B-yM_N)]}{M_B\sqrt{y}(1-y)}$
$+\frac{1}{2}$	-1	$-\frac{1}{\sqrt{3}}\frac{f}{M_V}\frac{k_R(-2M_NM_B(1-y)+yM_V^2)}{M_B\sqrt{y}(1-y)}$
$-\frac{1}{2}$	1	$\frac{1}{\sqrt{3}}\frac{f}{M_V}\frac{2M_B(1-y)k_\perp^2-M_B^3(1-y)^2+M_NM_V^2y^3}{M_By\sqrt{y}(1-y)}$
$-\frac{1}{2}$	0	$\sqrt{\frac{2}{3}}\frac{f}{M_V}\frac{M_Vk_R[M_Ny-(1-y)M_B]}{M_B\sqrt{y}(1-y)}$
$-\frac{1}{2}$	-1	$\frac{1}{\sqrt{3}}\frac{f}{M_V}\frac{M_Nk_R^2}{M_B\sqrt{y}(1-y)}$
$-\frac{3}{2}$	1	$\frac{f}{M_V}\frac{M_Bk_R(1-y)}{y\sqrt{y}}$
$-\frac{3}{2}$	0	0
$-\frac{3}{2}$	-1	0

TABLE VII. Vertex functions for $N \to \Delta V$ and particle helicities $\frac{1}{2} \to \lambda'$, λ_V in prescription B.

λ'	λ_V	$V(N, \Delta V)$
$+\frac{3}{2}$	$+1$	$-\frac{f}{M_V}\frac{k_L^2}{y\sqrt{y}(1-y)}$
$+\frac{3}{2}$	0	$-\frac{f}{M_V}\frac{k_L[k_\perp^2-yM_V^2-y(1-y)M_N^2+(1-y)M_B^2]}{\sqrt{2}M_Vy\sqrt{y}(1-y)}$
$+\frac{3}{2}$	-1	$\frac{f}{M_V}\frac{k_\perp^2+(1-y)(M_N+M_B)(M_B-yM_N)}{\sqrt{y}(1-y)}$
$+\frac{1}{2}$	1	$\frac{1}{\sqrt{3}}\frac{f}{M_V}\frac{k_L[k_\perp^2-2(1-y)M_B^2]}{M_By\sqrt{y}(1-y)}$
$+\frac{1}{2}$	0	$\frac{1}{\sqrt{6}}\frac{f}{M_V}\frac{[k_\perp^2+(1-y)M_B^2-y(1-y)M_N^2-yM_V^2)][k_\perp^2-(1-y)M_B^2+y(1-y)M_NM_B]}{M_BM_Vy\sqrt{y}(1-y)}$
$+\frac{1}{2}$	-1	$\frac{1}{\sqrt{3}}\frac{f}{M_V}\frac{k_R[-k_\perp^2+(1-y)(yM_N^2-2M_NM_B-M_B^2)]}{M_B\sqrt{y}(1-y)}$
$-\frac{1}{2}$	1	$\frac{1}{\sqrt{3}}\frac{f}{M_V}\frac{k_\perp^2[2M_B(1-y)-y^2M_N]+(1-y)[y^3M_N^3-M_NM_B^2y^2-M_B^3(1-y)]}{M_By\sqrt{y}(1-y)}$
$-\frac{1}{2}$	0	$\frac{1}{\sqrt{6}}\frac{f}{M_V}\frac{k_R[M_Ny-(1-y)M_B][y(1-y)M_N^2-(1-y)M_B^2+yM_V^2-k_\perp^2]}{M_BM_Vy\sqrt{y}(1-y)}$
$-\frac{1}{2}$	-1	$\frac{1}{\sqrt{3}}\frac{f}{M_V}\frac{M_Nk_R^2}{M_B\sqrt{y}(1-y)}$
$-\frac{3}{2}$	1	$\frac{f}{M_V}\frac{M_Bk_R(1-y)}{y\sqrt{y}}$
$-\frac{3}{2}$	0	0
$-\frac{3}{2}$	-1	0

The results of the calculation for the particle helicities $\frac{1}{2} \to \lambda'_N, \lambda_V$ are given in Table IV for prescription A and in Table V for prescription B.

The corresponding results for helicity down of the nucleon are given by

$$V^{-(1/2)(N,BV)}_{\lambda',\lambda_V}(y, \mathbf{k}_\perp) = (-1)^{1/2+\lambda'+\lambda_V} V^{1/2(N,BV)}_{-\lambda',-\lambda_V}(y, \hat{\mathbf{k}}_\perp),$$

where $\hat{\mathbf{k}}_\perp = (k_x, -k_y)$.

The vertex function for the transition $N \to BV$ with the baryon being one of the decuplet states is given by

$$V^{\lambda}_{\lambda',\lambda_V} = \tilde{\phi}^*_V \cdot \tilde{T} F_{NBV}(y, k_\perp) \frac{f}{M_V} \bar{u}_\nu(\tilde{p}'_B, \lambda') \gamma_5 \gamma_\mu \times u(\tilde{p}_N, \lambda)[p^\mu_V \varepsilon^{\nu*}_{\lambda_V} - p^\nu_V \varepsilon^{\mu*}_{\lambda_V}], \quad \text{(A9)}$$

where the isospin factor is defined as in Eq. (A7), with $T_B = \frac{3}{2}$ and $\langle \frac{1}{2} \| \hat{T} \| \frac{1}{2} \rangle = 2$.

The explicit results for particle helicities $\frac{1}{2} \to \lambda', \lambda_V$ are given in Table VI for prescription A and in Table VII for prescription B.

The corresponding results for helicity down of the nucleon are given by

$$V^{-(1/2)(N,BV)}_{\lambda',\lambda_V}(y, \mathbf{k}_\perp) = (-1)^{3/2+\lambda'+\lambda_V} V^{(1/2)(N,BV)}_{-\lambda',-\lambda_V}(y, \hat{\mathbf{k}}_\perp).$$

[1] R. Hofstadter, Annu. Rev. Nucl. Sci. **7**, 231 (1957).
[2] H. Gao, Int. J. Mod. Phys. E **12**, 1 (2003); **12**, 567(E) (2003).
[3] C. E. Hyde-Wright and K. de Jager, Annu. Rev. Nucl. Part. Sci. **54**, 217 (2004).
[4] J. Arrington, C. D. Roberts, and J. M. Zanotti, arXiv:nucl-th:0611050.
[5] C. F. Perdrisat, V. Punjabi, and M. Vanderhaeghen, Prog. Part. Nucl. Phys. **59**, 694 (2007).
[6] K. de Jager, AIP Conf. Proc. **904**, 95 (2007).
[7] M. Göckeler *et al.* (QCDSF/UKQCD Collaboration), Phys. Rev. D **71**, 034508 (2005).
[8] M. Göckeler *et al.* (QCDSF/UKQCD Collaboration), Proc. Sci., LAT2006 (2006) 160.
[9] C. Alexandrou, G. Koutsou, J. W. Negele, and A. Tsapalis, Phys. Rev. D **74**, 034508 (2006).
[10] S. Boinepalli, D. B. Leinweber, A. G. Williams, J. M. Zanotti, and J. B. Zhang, Phys. Rev. D **74**, 093005 (2006).
[11] E. G. Edwards *et al.* (LHPC Collaboration), Proc. Sci., LAT2006 (2006) 121.
[12] M. Diehl, Th. Feldmann, R. Jakob, and P. Kroll, Eur. Phys. J. C **39**, 1 (2005).
[13] C. Alexandrou, G. Koutsou, Th. Leontiou, J. W. Negele, and A. Tsapalis, arXiv:0706.3011.
[14] V. Bernard, H. W. Fearing, T. R. Hemmert, and Ulf-G. Meißner, Nucl. Phys. **A635**, 121 (1998); **A642**, 563 (1998).
[15] D. B. Leinweber, A. W. Thomas, and R. D. Young, Phys. Rev. Lett. **86**, 5011 (2001).
[16] T. R. Hemmert and W. Weise, Eur. Phys. J. A **15**, 487 (2002).
[17] Ulf-G. Meißner and G. Schierholz, arXiv:hep-ph/0611072.
[18] J. D. Ashley, D. B. Leinweber, A. W. Thomas, and R. D. Young, Eur. Phys. J. A **19**, 9 (2004).
[19] V. Punjabi *et al.* (Jefferson Lab Hall A Collaboration), Phys. Rev. C **71**, 055202 (2005); **71**, 069902(E) (2005).
[20] C. E. Carlson and M. Vanderhaeghen, arXiv:hep-ph/0701272.
[21] J. Arrington, W. Melnitchouk, and J. A. Tjon, arXiv:0707.1861.
[22] R. P. Feynman, *Photon-Hadron Interactions* (W. A. Benjamin, New York, 1972).
[23] J. D. Sullivan, Phys. Rev. D **5**, 1732 (1972).
[24] A. W. Thomas, Phys. Lett. **126B**, 97 (1983).
[25] J. J. Kelly, Phys. Rev. C **66**, 065203 (2002).
[26] J. Friedrich and Th. Walcher, Eur. Phys. J. A **17**, 607 (2003).
[27] H.-W. Hammer, Ulf-G. Meißner, and D. Drechsel, Phys. Lett. B **586**, 291 (2004).
[28] H.-W. Hammer and Ulf-G. Meißner, Eur. Phys. J. A **20**, 469 (2004).
[29] M. A. Belushkin, H.-W. Hammer, and Ulf-G. Meißner, Phys. Rev. C **75**, 035202 (2007).
[30] G. A. Miller, Phys. Rev. Lett. **99**, 112001 (2007).
[31] B. Kubis and Ulf-G. Meißner, Eur. Phys. J. C **18**, 747 (2001); Nucl. Phys. **A679**, 698 (2001).
[32] Th. Fuchs, J. Gegelia, and S. Scherer, J. Phys. G **30**, 1407 (2004).
[33] M. R. Schindler, J. Gegelia, and S. Scherer, Eur. Phys. J. A **26**, 1 (2005).
[34] S. D. Bass, D. Schütte, Z. Phys. A **357**, 85 (1997).
[35] Z. Dziembowski, H. Holtmann, A. Szczurek, and J. Speth, Ann. Phys. (N.Y.) **258**, 1 (1997).
[36] D. H. Lu, A. W. Thomas, and A. G. Williams, Phys. Rev. C **57**, 2628 (1998).
[37] Y. B. Dong, A. Faessler, and K. Shimizu, Eur. Phys. J. A **6**, 203 (1999).
[38] A. Faessler, Th. Gutsche, V. E. Lyubovitskij, and K. Pumsa-ard, Phys. Rev. D **73**, 114021 (2006).
[39] B. Juliá-Díaz and D. O. Riska, Nucl. Phys. **A780**, 175 (2006).
[40] Q. B. Li and D. O. Riska, Nucl. Phys. **A791**, 406 (2007).
[41] D. Y. Chen, Y. B. Dong, M. M. Giannini, and E. Santopinto, Nucl. Phys. **A782**, 62c (2007).
[42] J. P. B. C. de Melo, T. Frederico, E. Pace, S. Pisano, and G. Salmè, Nucl. Phys. **A782**, 69c (2007).

[43] S. D. Drell, D. J. Levy, and T.-M. Yan, Phys. Rev. D **1**, 1035 (1970).
[44] V. R. Zoller, Z. Phys. C **53**, 443 (1992).
[45] V. R. Zoller, Z. Phys. C **54**, 425 (1992).
[46] R. L. Jaffe and G. C. Ross, Phys. Lett. **93B**, 313 (1980).
[47] B. Pasquini and S. Boffi, Phys. Rev. D **73**, 094001 (2006).
[48] J. Speth and A. W. Thomas, Adv. Nucl. Phys. **24**, 83 (1998).
[49] W. Melnitchouk, J. Speth, and A. W. Thomas, Phys. Rev. D **59**, 014033 (1999).
[50] S. Boffi, B. Pasquini, and M. Traini, Nucl. Phys. **B649**, 243 (2003).
[51] F. Schlumpf, J. Phys. G **20**, 237 (1994).
[52] Ho-Meoyng Choi and Chueng-Ryong Ji, Phys. Rev. D **59**, 074015 (1999).
[53] S. J. Brodsky and G. P. Lepage, in *Perturbative Quantum Chromodynamics*, edited by A. H. Mueller (World Scientific, Singapore 1989).
[54] H. Holtmann, A. Szczurek, and J. Speth, Nucl. Phys. **A596**, 631 (1996).
[55] C. Boros and A. W. Thomas, Phys. Rev. D **60**, 074017 (1999).
[56] R. Machleidt, K. Holinde, and Ch. Elster, Phys. Rep. **149**, 1 (1987).
[57] M. Alberg, E. M. Henley, and G. A. Miller, Phys. Lett. B **471**, 396 (2000).
[58] W.-M. Yao *et al.* (Particle Data Group), J. Phys. G **33**, 1 (2006).
[59] S. D. Drell and T. M. Yan, Phys. Rev. Lett. **24**, 181 (1970).
[60] B. D. Keister and W. N. Polyzou, Adv. Nucl. Phys. **20**, 225 (1991).
[61] F. Cardarelli, E. Pace, G. Salmè, and S. Simula, Phys. Lett. B **357**, 267 (1995).
[62] R. Kreckel, Comput. Phys. Commun. **106**, 258 (1997); arXiv:physics/9710028.
[63] Z. Dziembowski, Phys. Rev. D **37**, 778 (1988).
[64] P. L. Chung and F. Coester, Phys. Rev. D **44**, 229 (1991).
[65] Bo-Qiang Ma, Di Qing, and I. Schmidt, Phys. Rev. C **65**, 035205 (2002).
[66] F. Cardarelli and S. Simula, Phys. Rev. C **62**, 065201 (2000).
[67] R. F. Wagenbrunn, S. Boffi, W. Klink, W. Plessas, and M. Radici, Phys. Lett. B **511**, 33 (2001).
[68] S. Boffi, L. Ya. Glozman, W. Klink, W. Plessas, M. Radici, and R. F. Wagenbrunn, Eur. Phys. J. A **14**, 17 (2002).
[69] B. Juliá-Díaz, D. O. Riska, and F. Coester, Phys. Rev. C **69**, 035212 (2004); arXiv:hep-ph/0312169.
[70] B. Juliá-Díaz, AIP Conf. Proc. **904**, 167 (2007).
[71] V. Bernard, L. Elouadrhiri, and Ulf-G. Meißner, J. Phys. G **28**, R1 (2002).
[72] A. I. L'vov, S. Scherer, B. Pasquini, C. Unkmeir, and D. Drechsel, Phys. Rev. C **64**, 015203 (2001).
[73] J. B. Kogut and D. E. Soper, Phys. Rev. D **1**, 2901 (1970); J. B. Kogut, Phys. Rev. D**5**, 1152 (1972).
[74] M. Burkardt, Phys. Rev. D **66**, 114005 (2002); Int. J. Mod. Phys. A **18**, 173 (2003).
[75] B. Pasquini and S. Boffi, Phys. Lett. B **653**, 23 (2007).
[76] F.-G. Cao and A. I. Signal, Eur. Phys. J. C **21**, 105 (2001).
[77] R. J. Fries and A. Schäfer, Phys. Lett. B **443**, 40 (1998). The momentum distributions are found in arXiv:hep-ph/9805509.
[78] S. Kumano and M. Miyama, Phys. Rev. D **65**, 034012 (2002).
[79] J. D. Bjorken and S. D. Drell, *Relativistic Quantum Fields* (McGraw-Hill, New York, 1965).
[80] D. Binosi and L. Theussl, Comput. Phys. Commun. **161**, 76 (2004).